

Article

Interactions of Perrhenate ($\text{Re(VII)}\text{O}_4^-$) with Fe(II)-Bearing Minerals

Anthony W. N. Kilber¹, Maxim I. Boyanov^{1,2} , Kenneth M. Kemner¹ and Edward J. O'Loughlin^{1,*} ¹ Argonne National Laboratory, Biosciences Division, Lemont, IL 60439-4843, USA; mboyanov@anl.gov or mboyanov@iche.bas.bg (M.I.B.); kemner@anl.gov (K.M.K.)² Institute of Chemical Engineering, Bulgarian Academy of Sciences, 1113 Sofia, Bulgaria

* Correspondence: oloughlin@anl.gov; Tel.: +1-630-252-9902

Abstract: Rhenium (Re) is an extremely rare element, with a crustal abundance of approximately 0.4 parts per billion (ppb) and a sea water concentration of 8.3 parts per trillion (ppt). However, Re concentrations in anoxic marine sediments range from 2 to 184 ppb, which is attributed to reduction of the highly soluble perrhenate ion ($\text{Re(VII)}\text{O}_4^-$) to insoluble Re(IV) species. Anoxic sediments typically contain Fe(II) and sulfide species, which could potentially reduce Re(VII) to Re(IV). In this study, we examined the interactions of KReO_4 with magnetite (Fe_3O_4), siderite (FeCO_3), vivianite ($(\text{Fe}_3(\text{PO}_4)_2 \bullet 8\text{H}_2\text{O})$), green rust (mixed Fe(II)/Fe(III) layered double hydroxide), mackinawite (FeS), and chemically reduced nontronite (NAu-1) using X-ray absorption near-edge structure (XANES) and extended X-ray absorption fine structure (EXAFS) spectroscopy to determine the valence state and speciation of Re. Uptake of Re by green rust was rapid, with ~50% associated with the solids within 2 days. In contrast, there was <10% uptake by the other Fe(II) phases over 48 days. Reduction of Re(VII) to Re(IV) was only observed in the presence of green rust, producing clusters of bidentate-coordinated $\text{Re(IV)}\text{O}_6$ octahedra. These results suggest that except for green rust, the potential for other Fe(II)-bearing minerals to act as reductants for ReO_4^- in sedimentary environments requires further investigation.



Citation: Kilber, A.W.N.; Boyanov, M.I.; Kemner, K.M.; O'Loughlin, E.J. Interactions of Perrhenate ($\text{Re(VII)}\text{O}_4^-$) with Fe(II)-Bearing Minerals. *Minerals* **2024**, *14*, 181. <https://doi.org/10.3390/min14020181>

Academic Editor: Jiří Sejkora
Received: 9 January 2024
Revised: 1 February 2024
Accepted: 3 February 2024
Published: 7 February 2024



Copyright: © 2024 by the authors. Licensee MDPI, Basel, Switzerland. This article is an open access article distributed under the terms and conditions of the Creative Commons Attribution (CC BY) license (<https://creativecommons.org/licenses/by/4.0/>).

1. Introduction

Rhenium (Re), element 75 on the periodic table, is one of the rarest elements on the Earth, with an average seawater concentration of 8.3 ppt and an average crustal abundance of approximately 0.4 ppb [1]. However, Re is enriched in anoxic marine sediments, with reported concentrations ranging from 2 to 184 ppb [2,3], and it is because of this high seawater-to-crustal abundance ratio that it is more enriched than any other metal [4]. Re has 10 valence states ranging from -3 to +7; however, +4 and +7 are the most geochemically relevant in the shallow subsurface [1,5]. In oxic environments, Re is typically present as the highly soluble perrhenate ion ($\text{Re(VII)}\text{O}_4^-$), and Re(IV) is thermodynamically stable under anoxic conditions (Figure 1) and may be found as sparingly soluble ReO_2 and ReS_2 in anoxic marine and lacustrine sediments [6,7]. The conservative behavior of Re(VII) in aquatic systems under oxic conditions [8] and the accumulation of Re in anoxic sediments have led to the use of Re as a paleoredox proxy [9–14].

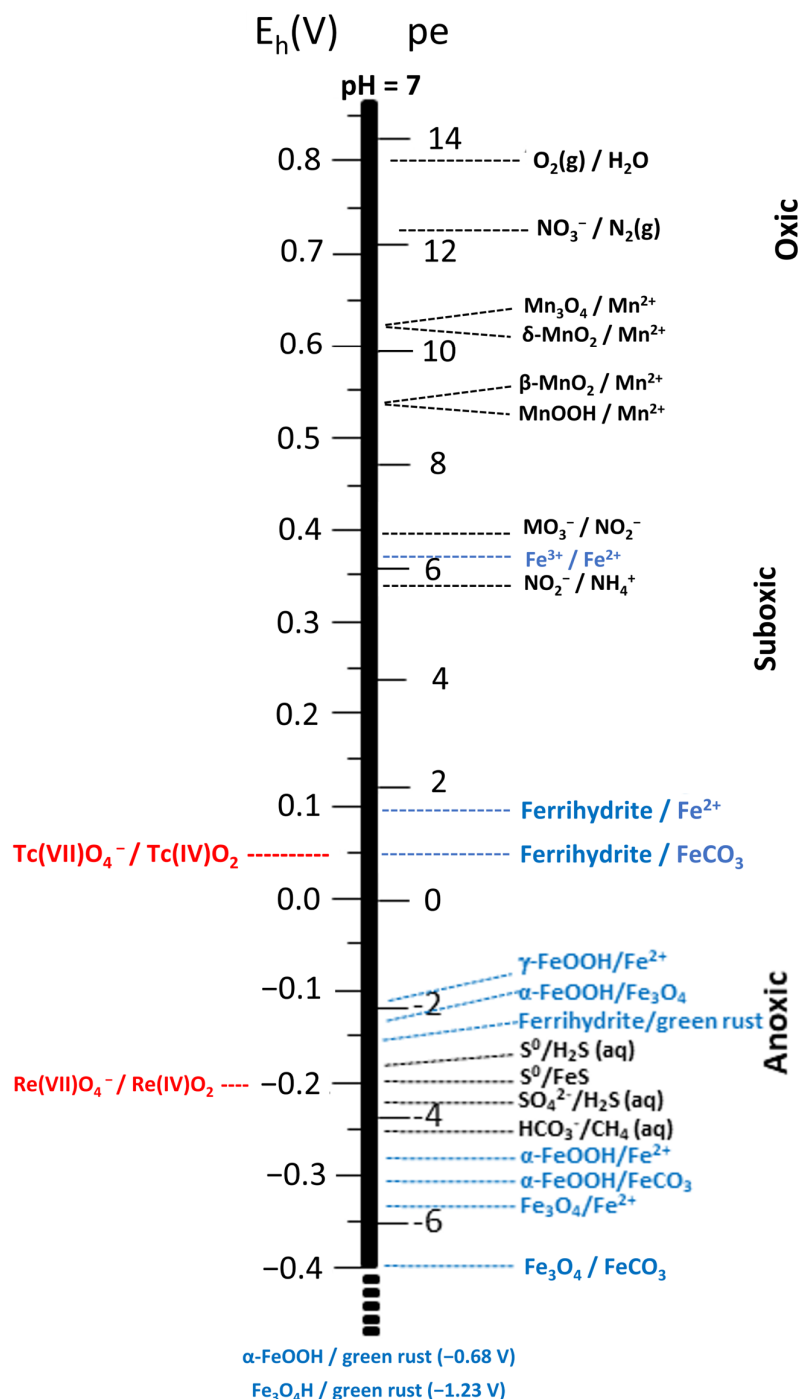


Figure 1. Redox ladder comparing the redox potentials of dominant biogeochemical electron donor–acceptor couples (emphasizing Fe(III)/Fe(II) couples) with reduction potentials of ReO_4^- / ReO_2 and TcO_4^- / TeO_2 couples. Reduction potentials of the dominant biogeochemical couples were obtained from Langmuir [15] and Thandrum [16] (in black) and Amonette [17] (in blue) under the conditions identified therein. The reduction potentials for Re and Tc couples (in red) at $10^{-8}\ M$ aqueous Re or Tc, $I = 0$, and $298.15\ K$ were calculated from thermodynamic data from Wagman et al. [18] and Rard et al. [19], respectively.

The mechanism of Re enrichment in anoxic sediments is not well defined but is presumed to involve the reduction of $Re(VII)$ to $Re(IV)$ [2,4,6,7,20]; however, there are proposed mechanisms that could result in accumulation of $Re(VII)$ species in sediments under euxinic (anoxic and sulfidic) conditions [21]. Correlation of Re content with organic

carbon in black shales [22,23] could be an indication that reduction of Re(VII) to Re(IV) in sediments is driven by microbial activity. Indeed, direct enzymatic reduction of metals and metalloids by bacteria has been demonstrated for a broad range of elements that are redox-active under anoxic conditions in surficial aquatic and terrestrial environments [24], including reduction of Tc(VII) to Tc(IV) [25]. Since Re is often studied as a nonradioactive geochemical analog of highly radioactive Tc [25], perhaps studies of the microbial reduction of Tc(VII) might provide insights into pathways for Re(VII) reduction. However, Dolor et al. [26] saw no direct evidence of Re(VII) reduction by the Fe(III)-reducing bacteria *Geobacter metallireducens* GS-15 and *Shewanella oneidensis* MR-1 and the sulfate-reducing bacterium *Desulfovibrio desulfuricans*, all of which can reduce Tc(VII) to Tc(IV) [27,28]. Anoxic sediments typically contain Fe(II) and sulfide species, many of which could be electron donors for the reduction of Re(VII) to Re(IV) (Figure 1), and several Fe(II)-bearing minerals and sulfide species are effective at reducing Tc(VII) to Tc(IV) [29]; however, their potential for reduction of Re(VII) has not been well studied. Reduction of Re(VII) to Re(IV) has been observed during coprecipitation of mackinawite (FeS) and during the interaction of perrhenate with pyrite [30–32]; however, the potential for Re(VII) reduction by other Fe-bearing minerals has not been reported.

The objective of this study was to assess the potential for reduction of Re(VII) to Re(IV) by Fe(II)-bearing minerals by examining the interaction of $\text{Re}(\text{VII})\text{O}_4^-$ (500 μm) in aqueous suspensions containing 25 mM Fe(II) as green rust (mixed Fe(II)/Fe(III) layered double hydroxide), mackinawite, magnetite (Fe_3O_4), siderite (FeCO_3), vivianite [$\text{Fe}_3(\text{PO}_4)_2 \bullet 8\text{H}_2\text{O}$], or structural Fe(II) in an Fe-rich smectite, all of which are minerals containing Fe(II) that are commonly observed products of the bioreduction of Fe(III) phases and are found in lacustrine and marine sediments [33–35]. The chemical speciation and valence state of Re were determined using X-ray absorption spectroscopy (XAFS) [36].

2. Materials and Methods

Aqueous suspensions of mackinawite, magnetite, siderite, sulfate green rust, and vivianite were prepared as described by Johnson et al. [37]. The citrate–bicarbonite–dithionite method as used to reduce structural Fe(III) to Fe(II) in NAu-1 (a green-colored, Al-enriched nontronite from Uley Mine, South Australia obtained from the Clay Minerals Society’s Source Clays Repository [<http://www.clays.org/> (accessed on 27 October 2023)] [38]. All mineral stock suspensions were buffered at pH 7.2 in 20 mM 3-morpholinopropane-1-sulfonic acid (MOPS).

The interaction of Re(VII) with Fe(II) minerals was investigated in 160 mL serum bottles containing 120 mL of 20 mM MOPS buffer at pH 7.2 amended with 500 μM KReO_4 and 25 mM Fe(II) as either green rust, mackinawite, magnetite, siderite, vivianite, or chemically reduced nontronite. The experimental systems were prepared and sealed with butyl rubber plugs and aluminum crimp caps in a glove box (Coy Laboratory Products, Grass Lake, Michigan) with an atmosphere containing 3%–5% H_2 in N_2 , using a Pd catalyst to maintain <1 ppm O_2 at all times. The bottles were placed on a roller drum and maintained in the dark at 25 °C. Subsamples were removed from the experimental systems at designated times using a needle and a syringe and filtered through 25 mm-diameter 0.2 μm -pore-size nylon filters. Concentrated HCl was added to acidify the samples to pH 1 to preserve the samples prior to the determinations of aqueous Re concentration by inductively coupled plasma-optical emission spectroscopy (ICP-OES) using a PerkinElmer 4300DV instrument (PerkinElmer Inc., Waltham, MA, USA). The Re emission line at 297.248 nm was measured in the radial view mode, which provided a detection limit of 0.5 μM Re. Samples for Re XAFS analysis were prepared by placing the solids that were retained on the filter in a 1.5 mm thick Plexiglas sample holder with Kapton windows. Sample collection and processing were conducted under anoxic conditions using the glove box described above.

Re L_{III}-edge (10,535 eV) XAFS measurements were conducted at the MR-CAT/Enviro CAT bending magnet beamline (Sector 10, Advanced Photon Source) [39]. X-ray absorption near edge spectra (XANES) and extended X-ray absorption fine structure (EXAFS) spectra

were collected using gas-filled ionization chambers (transmission mode) or a four-element Vortex detector (fluorescence mode). Spectra were collected at room temperature inside a N₂-purged sample cell. Energy calibration was established by setting the inflection point in the spectrum from a Re metal sample to 10,535 eV. Energy calibration was maintained by collecting data from the reference metal simultaneously with the collection of data from the samples. Radiation-induced changes in the spectra were not detected. No differences were observed between spectra from three fresh areas on the sample, so all scans from each sample were averaged to produce the final spectrum. The speciation of Re in the suspension solids was determined by comparisons of the spectra to standards (polycrystalline NH₄ReO₄, ReO₃, ReO₂, and Re metal) mounted on the sticky side of a Kapton tape and measured previously at the same beamline [40]. A standard of Re(VII) sorbed on ferrihydrite was prepared by equilibrating a suspension of ferrihydrite (50 mM Fe(III)) with 20 mM ReO₄[−] for 30 days at 25 °C, after which the hydrated solids were collected by centrifugation and placed in a Plexiglas sample holder as previously described. An aqueous Re(VII) standard was prepared from a 0.1 M solution of NH₄ReO₄ [40].

3. Results and Discussion

3.1. Re Uptake by Fe(II)-Bearing Minerals

With the exception of green rust, uptake of Re by the Fe(II) minerals was <10% over a period of 48 days (Figure 2), the majority of which occurred within the first 12 days in all but the Re + FeS system. In the Re + green rust system, ~50% of the added Re partitioned to the solids within 2 days, but there was no additional uptake during the remainder of the experiment (48 days).

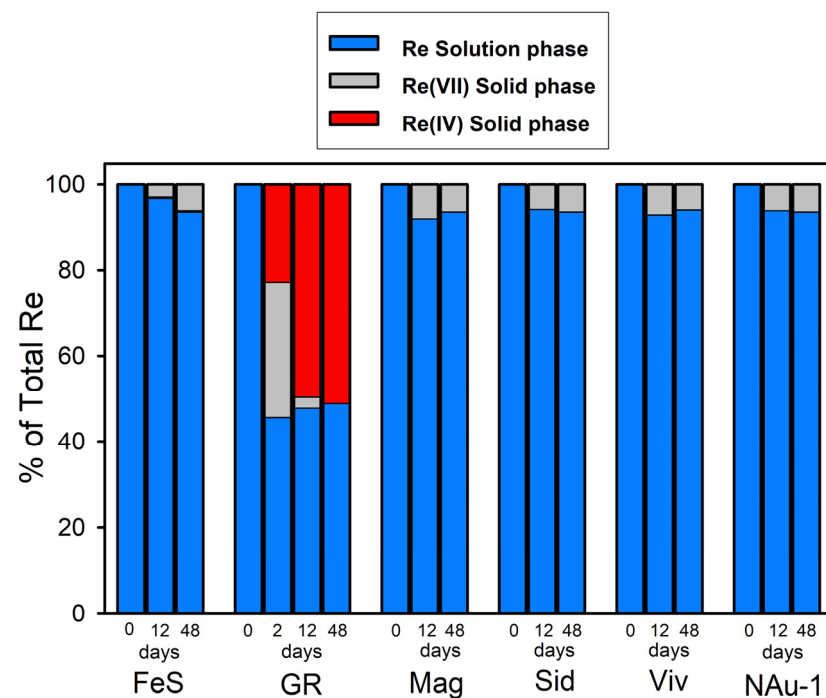


Figure 2. Distribution of Re among the solid and solution phases in the Fe(II) mineral suspensions to which 500 μ M Re(VII) was added. The proportion of solid-phase Re as Re(VII) or Re(IV) was determined by linear combination fits of the Re XANES spectra. The uncertainty reported by the fitting program was less than $\pm 5\%$. FeS—mackinawite; GR—sulfate green rust; Mag—magnetite; Sid—siderite; Viv—vivianite; NAu-1—chemically reduced nontronite.

3.2. Chemical Speciation of Mineral-Associated Re

3.2.1. Average Valence State of Re in the Solids (XANES)

Figure 3A compares the Re L_{III}-edge XANES spectra from the solids in the experimental systems to the ferrihydrite-adsorbed Re(VII) standard and the ReO₂ Re(IV) standard. The edge position and features clearly indicated that Re associated with magnetite, vivianite, siderite, FeS, and NAu-1 remains as Re(VII), i.e., no reduction was observed over the 48 day duration of the experiment. Linear combination fits of the data determined 100% ($\pm 5\%$) Re(VII) content in the samples).

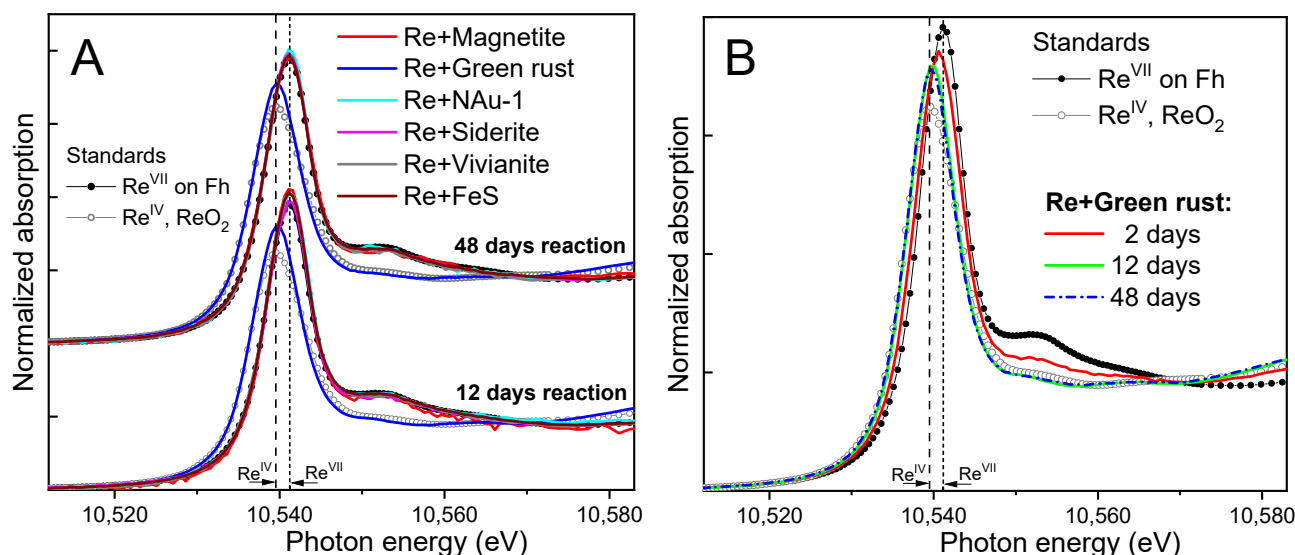


Figure 3. (A) Re L_{III}-edge XANES data from the reactor solids after 48 and 12 days of incubation (lines), compared to standards (symbols) of Re(VII) adsorbed on ferrihydrite (Fh) and a Re(IV) mineral, ReO₂. Vertical dashed lines indicate the differences in white line positions of the Re(IV) and Re(VII) standards. All experimental spectra overlay the Re(VII) standard, except that from the Re + green rust system which overlays the Re(IV) standard. (B) Reaction kinetics in the Re + green rust system, showing an intermediate reduction extent for the sample taken at 2 days and complete reduction to Re(IV) at 12 and 48 days.

Re(VII) was only reduced when reacted with green rust. The 12- and 48-day samples showed an edge position that was consistent with the Re(IV) standard ReO₂. However, there were shape and amplitude differences in the XANES between the samples and the ReO₂ standard, suggesting a different speciation of Re(IV) in the green rust system. The speciation differences were more clearly observable in the EXAFS data, which are presented in Section 3.2.3. To explore the short-term kinetics of Re(VII) reduction by green rust, an additional sample was measured after 2 days of reaction. The spectrum showed an intermediate valence state, which was quantified by linear combination fits with the two standards as 42% ($\pm 5\%$) Re(IV) and 58% Re(VII). After 12 days, the reduction was nearly complete at 95% ($\pm 5\%$) Re(IV), and the 48-day sample contained 100% ($\pm 5\%$) Re(IV). Thus, under the conditions of our study, green rust was able to reduce the solids-associated Re(VII) to Re(IV) within 2–12 days.

3.2.2. Local Atomic Coordination around Re(VII) (EXAFS)

Figure 4 shows the L_{III}-edge EXAFS spectra of the Re(VII) associated with the reduced Fe solids (EXAFS data for Re in the magnetite system were not collected due to beamtime constraints). All data overlay each other and the Re(VII) standards, indicating a similar coordination environment around Re. The data for Re + siderite, Re + vivianite, and Re+NAu-1 had a higher noise level, but also followed the adsorbed Re(VII) standard in phase and in amplitude, so the analysis below can be assumed applicable to those data as

well—albeit with higher uncertainty. The main peak near 1.4 Å in the Fourier transform (Figure 4B) is due to the tetrahedral O shell in the perrhenate anion $\text{Re(VII)}\text{O}_4^-$, and its similarity between the samples and the aqueous standard indicated that the structure of the perrhenate anion was not disturbed. In addition, there were no peaks between $R + \Delta = 1.7$ and 4.0 Å relative to the aqueous standard where atoms from complexed ligands may contribute in the spectrum. The lack of outer-shell features, together with the undisturbed O_4 shell, suggests an outer-sphere association of ReO_4^- with the solids. This binding mechanism is similar to prior findings of Re(VII) adsorbed outer-sphere to a Pd/C catalyst [40] but in contrast to Re(VII) adsorbed onto a siliceous zeolite where the main O peak showed a decreased amplitude indicative of a disturbance due to an inner-sphere monodentate complex [41]. A bidentate complexation mechanism can be excluded here, as the more rigid coordination and better-defined Re-Fe distances would result in contributions from the surface Fe atoms (Figure 4C). Thus, the EXAFS data suggest outer-sphere association of the unreduced perrhenate anions with ferrihydrite, siderite, vivianite, NAu-1, and FeS.

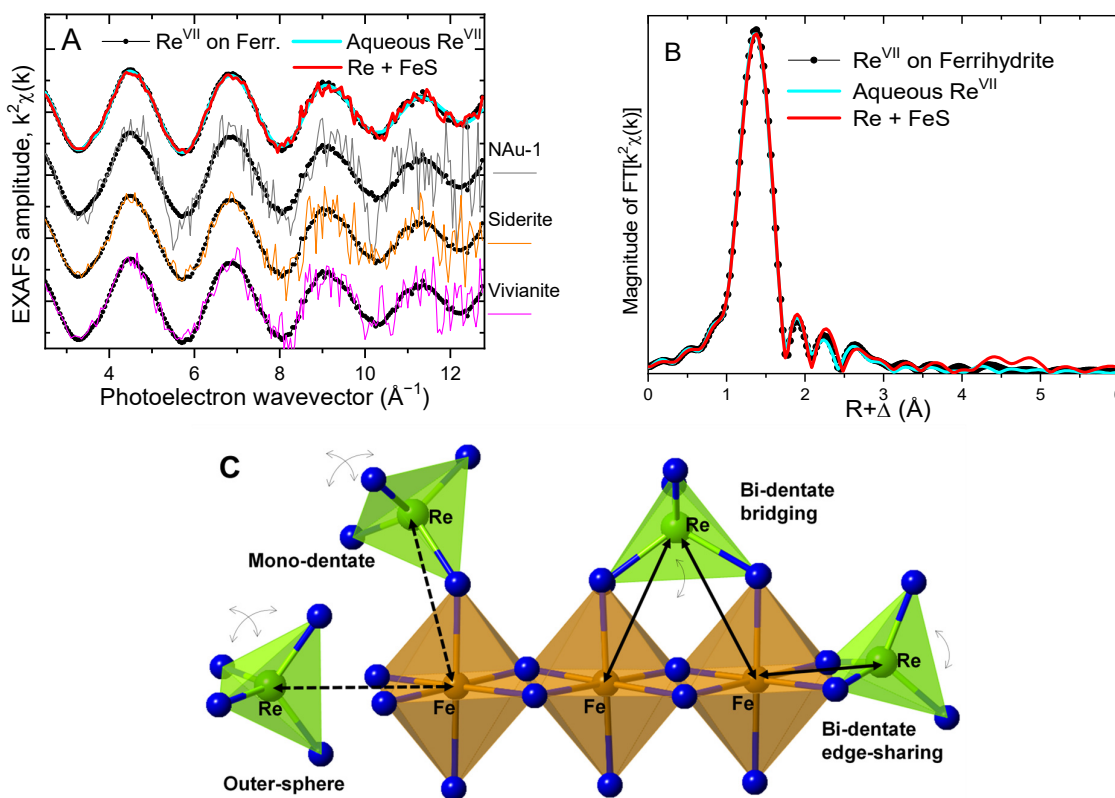


Figure 4. (A) Re L_{III}-edge EXAFS data from the samples in which no reduction occurred. The top graph shows the highest quality spectrum from the Re + FeS system, overlaid on the aqueous and the ferrihydrite-adsorbed Re(VII) standards. Below them, the spectra from Re(VII) associated with NAu-1, siderite, and vivianite were compared to the Re(VII) standard. (B) Fourier transforms of the top spectra in panel (A). (C) Structural models of Re(VII) adsorption to the mineral surface. Curved arrows illustrate the rotational freedom of the perrhenate anion in the different complexes. The Re-Fe distances are correspondingly better-defined in the bi-dentate complexes (solid arrows) and signals from the coordinating atoms appear in the EXAFS. The Re–Fe distances change over a broader range in the looser outer sphere and the monodentate complexes (dashed arrows), so signals from such atomic coordination are expected to lack coherence and not appear in the EXAFS.

3.2.3. Local Atomic Coordination around Re(IV) (EXAFS)

Figure 5 shows the L_{III}-edge EXAFS of Re(IV) associated with the green rust solids after 48 days, compared to the ReO₂ standard. The main peak near $R + \Delta = 1.6 \text{ \AA}$ in the Fourier transform (FT) is due to the octahedral O₆ coordination around Re(IV) [40]. Differences from the standard can be seen in the amplitude and position of this peak, in the outer-shell features, and in the shape and phase of the $\chi(k)$ signal, all of which indicate that the Re(IV) atoms in the green rust system were not precipitated as ReO₂. The presence of outer-shell peaks in the FT suggests the formation of an ordered structure, such as an agglomerate or an inner-sphere adsorption complex.

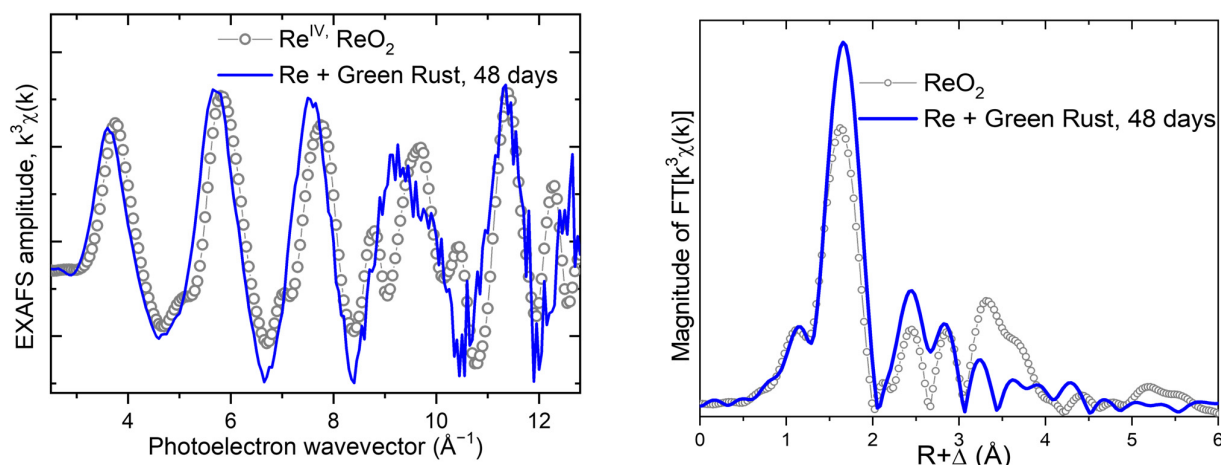


Figure 5. Re L_{III}-edge EXAFS data from the ReO₂ standard and the green rust sample after 48 days of reaction.

Further insights on the Re(IV) species were obtained in shell-by-shell fits of the data. The photoelectron scattering paths calculated by FEFF8 were calibrated in fits of the ReO₂ standard using its known crystal structure [42–44]. A four-shell, single-scattering model reproduced the main features of the ReO₂ data, where signals from both the bidentate Re-Re coordination ($R = 2.57 \text{ \AA}$), as well as monodentate Re-Re coordination ($R = 3.67 \text{ \AA}$), were needed to fit the data (Figure 6 and Table 1). Analysis of the Re+green rust data at 48 days using the same structural model reveals that the near-neighbor O bonds were slightly elongated ($R = 2.03 \text{ \AA}$) and less disordered (i.e., smaller σ^2) relative to ReO₂, suggesting a more relaxed and ordered ReO₆ octahedron than in the crystal structure. The FT peak near $R + \Delta = 2.4 \text{ \AA}$ is best reproduced by a Re shell at a distance of 2.59 \AA , which is consistent with bidentate edge-sharing coordination to 3 or 4 ReO₆ octahedra (Figure 6D). The rest of the FT peaks up to $R + \Delta = 3.5 \text{ \AA}$ were best reproduced by O shell contributions, presumably from the O atoms in the coordinated ReO₆ octahedra. Attempts to fit these peaks with Re shells were unsuccessful, so monodentate coordination (with characteristic Re-Re distances of $\sim 3.7 \text{ \AA}$, as in the ReO₂ structure) can be excluded. The alternative possibility of the peak near $R + \Delta = 2.4 \text{ \AA}$ being due to an Fe atom in a bidentate adsorption complex with the surface was also explored but resulted in a significantly worse fit. Therefore, the analysis of the EXAFS data suggests that Re(VII) reduced by green rust polymerizes in bidentate edge-sharing Re clusters (Figure 6D). Similar edge-sharing ReO₆ agglomerates have been observed, when Re(VII) was reduced by H₂ in the presence of Pd/C catalysts and on the surface of γ -alumina [45].

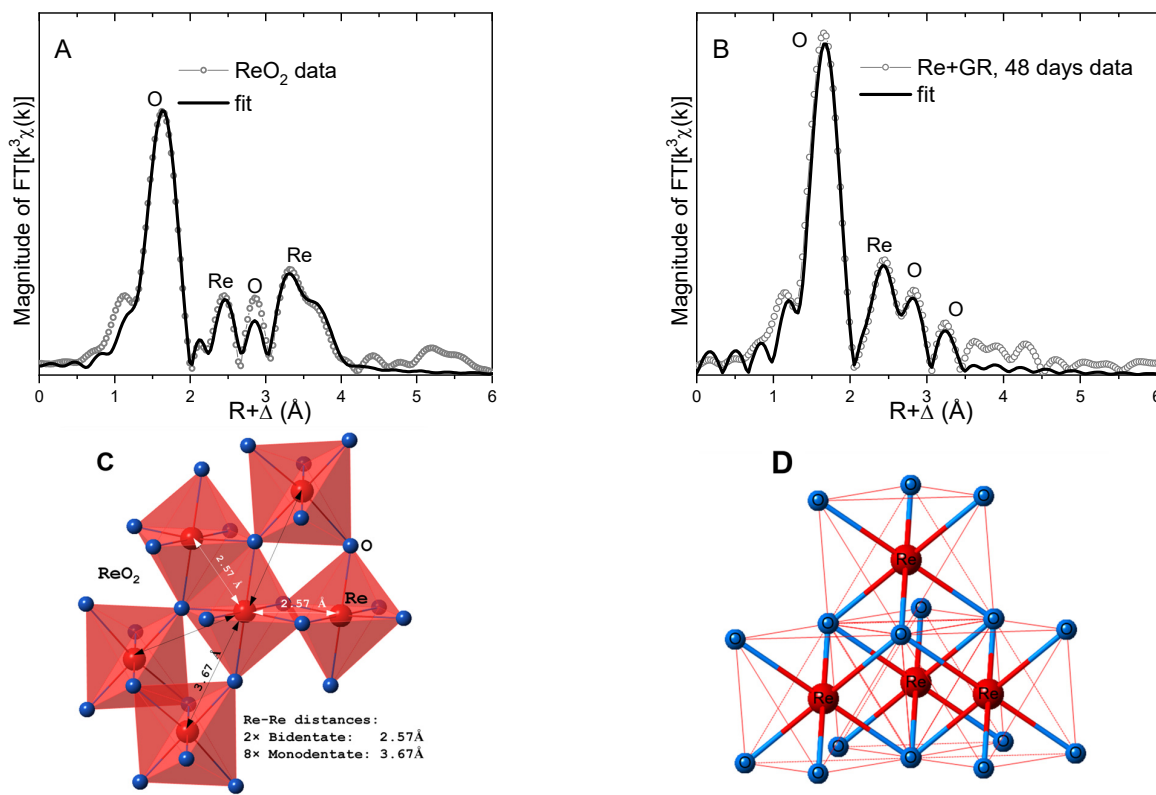


Figure 6. (A) Fit of the EXAFS data from the ReO_2 standard. (B) Fit of the data from Re(IV) associated with the green rust solids after 48 days; the numerical parameters are summarized in Table 1. (C) Partial structure of ReO_2 , illustrating the bidentate- and monodentate-coordinated Re octahedra and the corresponding Re–Re distances. (D) Illustration of the bidentate-coordinated Re agglomerate that is consistent with the fit of the EXAFS data from the reduced Re species in the green rust system.

Table 1. Numerical parameters for the fits in Figure 6.

Shell	N	R (Å)	σ^2 (Å ²)	ΔE (eV)	D	R-Factor
(A) ReO_2 standard						
O	6.0 ^a	1.99 ± 0.01	0.0046 ± 0.0009	6.0 ± 2.9	4	0.0125
Re	2.0 ^a	2.57 ± 0.01	0.0075 ± 0.0013			
O ^b	7.8 ± 3.6	3.67 ± 0.02	0.0033 ± 0.0037			
Re	8.0 ^a	3.69 ± 0.01	0.0082 ± 0.0017			
(B) Re reacted with green rust for 48 days						
O	6.0 ^a	2.03 ± 0.01	0.0025 ± 0.0005	5.5 ± 1.6	4	0.0128
Re	3.5 ± 1.3 ^c	2.58 ± 0.01	0.0066 ± 0.0021			
O	3.5 ^c	3.11 ± 0.04	0.0075 ± 0.0060			
O	7.0 ^c	3.69 ± 0.07	0.0146 ± 0.0120			

^a Coordination numbers were fixed to those in the structure of ReO_2 [44]. The refined S_0^2 factor was 0.84 ± 0.09 and was fixed to this value in the remaining fits. ^b This path was used to mimic the combined effects of single- and multiple-scattering contributions in the spectral region $R + \Delta = 2.8$ Å. As can be seen from the fit, the O shell used only partially reproduced the spectrum but served the purpose of interacting with the larger contributions from the surrounding Re atoms and helped their parametrization. ^c The coordination numbers for the outer O shells were constrained to vary as $1 \times N_{\text{Re}}$ and $2 \times N_{\text{Re}}$; otherwise, the correlation between N and σ^2 could not be resolved and led to unphysical values for these parameters. The rationale for the constraints is that the farther O signals were due to ReO_6 octahedra coordinated around the central Re, with fewer O atoms at close distances and more O atoms at farther distances. Other coefficients also reproduced the data well (e.g., $2 \times 4 \times N_{\text{Re}}$), so the coordination numbers of the O shells could not be defined by the fits.

4. Discussion

4.1. Reactivity of the Fe(II)-Bearing Minerals with Re(VII)

Among the Fe(II)-bearing minerals examined in this study, green rust was the most reactive, both in terms of uptake from solutions as well as reduction of Re(VII) to Re(IV). Green rusts are layered Fe(II)–Fe(III) hydroxides with a pyroaurite-type structure, consisting of alternating positively charged Fe(II)–Fe(III) hydroxide layers and hydrated anion layers, with the general composition— $[Fe(II)_{1-x} Fe(III)_x (OH)_{12}]^{x+} [(A)_{2/n} yH_2O]^{x-}$, where x typically ranges from 0.25 to 0.33, A is an n -valent anion (e.g., CO_3^{2-} , SO_4^{2-} , or Cl^-), and y denotes varying amounts of interlayer water (typically 2–4) [33]. Green rusts are key components of the biogeochemical cycling of Fe in aquatic and terrestrial systems [33] and are formed during direct microbial or coupled biotic/abiotic oxidation of Fe(II) under anoxic conditions by denitrifying bacteria [46–49], during microbial reduction of Fe(III) oxides [50–60], and during abiotic and microbially induced corrosion of iron and steel [61–64]. The enhanced uptake of Re by green rust observed in our study may be because, as an anion, perrhenate may have been able to sorb to green rust by anion exchange with sulfate (the green rust used in this study had sulfate as the interlayer anion). Uptake of Re(VII) by green rust was followed by reduction to Re(IV), which is consistent with the fact that green rusts are highly redox active and have been shown to be effective electron donors for the reduction of a wide range of nonmetals (N(V) and Cl(V)), transition metals (Ag(I), Au(III), Cr(VI), Cu(II), Hg(II), Pd(II), and Pt(IV)), metalloids (Se(VI/IV) and Te(VI/IV)), and radionuclides (Np(V), Tc(VII), and U(VI)) [65–78].

Uptake of Re from solutions by the other Fe(II)-bearing minerals examined in this study was limited (<10%), and there was no indication of reduction to Re(IV) over the timescale of our experiment (48 days). Given that the interaction of Re(VII) with Fe(II)-bearing minerals has been largely unexplored (i.e., ours is the first study to examine the interaction of ReO_4^- with green rust, siderite, magnetite, vivianite, mackinawite, and Fe(II)-bearing smectite under environmentally relevant conditions), there is a limited basis on which our results can be discussed in the context of previous studies. Wharton et al. [30] reported the reduction of Re(VII) to Re(IV) as an Re–S–Fe phase during coprecipitation with FeS; however, the experimental system is fundamentally different from our study. The study by Wharton et al. involved the addition of a solution of Na_2S to a solution containing $FeSO_4$ and ReO_4^- buffered at pH 4, while in our study, ReO_4^- was added to an aqueous suspension of pre-formed FeS buffered at pH 7.2. Ding et al. [31] examined the interaction of ReO_4^- with natural (geogenic) pyrite (FeS_2) and reported substantial uptake (~40%) at pH 12 and lower uptake (<20%) at $pH \leq 6.6$, with reduction to ReO_2 . Wang et al. [32] reported reduction of Re to ReO_2/ReS_2 by synthetic pyrite; however, in their study, the most effective removal of Re occurred at pH 3.5, with the pseudo-second order rate constant decreasing by a factor of 10.33 with increasing pH over a pH range of 3.5–9.0. The opposing pH effects on ReO_4^- uptake and reduction by natural and synthetic pyrite reported by Ding et al. and Wang et al. highlights how poorly we understand the processes controlling the interactions of Re with Fe(II)-bearing minerals.

4.2. Comparison of the Reactivity of Re and Tc

Given the hazards in working with highly radioactive Tc, Re has been studied as a nonradioactive geochemical analog of Tc (e.g., [79–81]), as they are both Group 7 elements, Re is one row above Te in the periodic table, and they share some physical and chemical properties [82]. For example, under oxic conditions and within the pH range typical of most natural aquatic environments, Re and Tc are present as septivalent soluble anionic species, perrhenate and pertechnetate (TcO_4^-), respectively. However, largely due to environmental and human health concerns related to the release of ^{99}Tc to the environment from radioactive wastes and fallout from fission bomb explosions, more is known about the biogeochemical behavior of Tc than Re [25,29,83–85], so perhaps our understanding of the interactions of Re with Fe(II)-bearing minerals can be informed by the behavior of Tc.

Unfortunately, this does not appear to be the case. Previous studies have demonstrated reduction of TcO_4^- to Tc(IV) phases (typically TcO_2 or TcS_2) by green rust [70], magnetite [86–88], siderite [87,89], vivianite [89], NAu-2 nontronite [90,91], and ferrous sulfide phases [87,88,92–94]. Of these Fe(II)-bearing minerals shown to reduce Tc(VII) , only green rust (this study) and pyrite [31,32] have been directly shown to reduce ReO_4^- to Re(IV) . Moreover, recalcitrance of ReO_4^- to chemical and biological reduction under conditions where Tc is readily reduced has been reported in many experimental systems (e.g., [26,82,95–97]). The differences in the redox behavior of Tc vs. Re are likely due, in part, to the difference in the $\text{Tc(VII)}/\text{Tc(IV)}$ and $\text{Re(VII)}/\text{Re(IV)}$ reduction potentials (Figure 1). The substantial differences in the redox reactivity of Re(VII) and Tc(VII) indicate that Re is not a good proxy for Tc in processes involving redox transformations.

4.3. Implications for Re Biogeochemistry

The objective of this study was to assess the potential for reduction of Re(VII) to Re(IV) by Fe(II)-bearing minerals that are commonly observed products of the microbial reduction of Fe(III) phases and are found in lacustrine and marine sediments. Our results indicate that green rust could be a potential reductant for ReO_4^- in sedimentary environments, as it is found in Fe(II)/Fe(III) transition zones across a broad range of aquatic and terrestrial environments [33]. Indeed, green rusts are believed to have played a central role in Fe cycling in Precambrian oceans and the development of iron formations [98], and possibly even the emergence of life on Earth [99,100]. As such, they could play a role in the fixation of Re in marine sediments under ferruginous conditions (Fe-rich, anoxic conditions that have been a dominant feature of the deep ocean throughout much of Earth's history [101]).

The apparent lack of reactivity of the other Fe(II)-bearing phases examined in this study does not necessarily preclude their involvement in Re reduction in sediments. Cruius and Thomson [102] suggested that the depth distribution profiles of Re in marine sediments from the Madeira Abyssal Palin may have been the result of kinetic limitations on the reduction of ReO_4^- to Re(IV) due to a multistep reduction reaction with slow kinetics at one or more of the electron transfers. Similarly, Sundby et al. [103] invoked slow kinetics for the reductive immobilization of ReO_4^- to explain the depth distribution profiles of Re in sediments from the Laurentian Trough. Yamashita et al. [6] suggested that slow reduction kinetics limited the extent of ReO_4^- reduction to Re(IV) in laboratory incubations of marine sediments even though the thermodynamics for the reaction were highly favorable. Indeed, depending on the geochemical conditions (pH, temperature, and solution phase concentrations of relevant Fe and Re species), reduction of Re(VII) to Re(IV) is thermodynamically favorable for other Fe(II) species/phases in addition to green rust. Therefore, it is possible that reduction of ReO_4^- in our experimental system by Fe(II) phases other than green rust may have been observed with a longer reaction period. As such, further studies are needed to better determine the potential involvement of Fe(II) phases in the reduction of ReO_4^- in sedimentary environments over longer timescales as well as under a broader range of geochemical conditions.

Author Contributions: Conceptualization, E.J.O.; formal analysis, M.I.B.; funding acquisition, M.I.B., K.M.K. and E.J.O.; investigation, A.W.N.K., M.I.B., K.M.K. and E.J.O.; project administration, E.J.O.; visualization, M.I.B.; writing—original draft, A.W.N.K., M.I.B. and E.J.O.; writing—review and editing, A.W.N.K., M.I.B., K.M.K. and E.J.O. All authors have read and agreed to the published version of the manuscript.

Funding: Research under the Wetlands Hydrobiogeochemistry Scientific Focus Area (SFA) at Argonne National Laboratory was supported by the Environmental Systems Science Program, Office of Biological and Environmental Research (BER), Office of Science, U.S. Department of Energy (DOE), under contract DE-AC02-06CH11357. MR-CAT/EnviroCAT operations are supported by DOE and the member institutions. Use of the Advanced Photon Source, an Office of Science User Facility operated for the U.S. Department of Energy (DOE) Office of Science by Argonne National Laboratory, was supported by the U.S. DOE under Contract No. DE-AC02-06CH11357. Argonne National Laboratory is a U.S. Department of Energy laboratory managed by UChicago Argonne, LLC. This work was

supported in part by the U.S. DOE, Office of Science, Office of Workforce Development for Teachers and Scientists (WDTS) under the Science Undergraduate Laboratory Internship Program (SULI).

Data Availability Statement: Data available on request due to internal policy and future research.

Acknowledgments: We thank the MR-CAT/EnviroCAT beamline staff for assistance during data collection at the synchrotron and the anonymous reviewers for their thoughtful reviews of the manuscript.

Conflicts of Interest: The authors declare no conflict of interest. The funders had no role in the design of the study; in the collection, analyses, or interpretation of data; in the writing of the manuscript, or in the decision to publish the results.

References

- John, D.A.; Seal, R.R., II; Polyak, D.E. Rhenium. In *Critical Mineral Resources of the United States—Economic and Environmental Geology and Prospects for Future Supply: U.S. Geological Survey Professional Paper 1802-P*; Schulz, K.J., DeYoung, J.H., Jr., Seal, R.R., II, Bradley, D.C., Eds.; Government Printing Office: Washington, DC, USA, 2017; pp. P1–P49. [[CrossRef](#)]
- Koide, M.; Hodge, V.F.; Yang, J.S.; Stallard, M.; Goldberg, E.G.; Calhoun, J.; Bertine, K.K. Some comparative marine chemistries of rhenium, gold, silver and molybdenum. *Appl. Geochem.* **1986**, *1*, 705–714. [[CrossRef](#)]
- Ravizza, G.; Turekian, K.K.; Hay, B.J. The geochemistry of rhenium and osmium in recent sediments from the Black Sea. *Geochim. Cosmochim. Acta* **1991**, *55*, 3741–3752. [[CrossRef](#)]
- Colodner, D.; Sachs, J.; Ravizza, G.; Turekian, K.; Edmond, J.; Boyle, E. The geochemical cycle of rhenium: A reconnaissance. *Earth Planet. Sci. Lett.* **1993**, *117*, 205–221. [[CrossRef](#)]
- Tagami, K.; Uchida, S. *Rhenium. Encyclopedia of Inorganic and Bioinorganic Chemistry*; John Wiley & Sons, Inc.: Hoboken, NJ, USA, 2011. [[CrossRef](#)]
- Yamashita, Y.; Takahashi, Y.; Haba, H.; Enomoto, S.; Shimizu, H. Comparison of reductive accumulation of Re and Os in seawater–sediment systems. *Geochim. Cosmochim. Acta* **2007**, *71*, 3458–3475. [[CrossRef](#)]
- Chappaz, A.; Gobeil, C.; Tessier, A. Sequestration mechanisms and anthropogenic inputs of rhenium in sediments from Eastern Canada lakes. *Geochim. Cosmochim. Acta* **2008**, *72*, 6027–6036. [[CrossRef](#)]
- Anbar, A.D.; Creaser, R.A.; Papanastassiou, D.A.; Wasserburg, G.J. Rhenium in seawater: Confirmation of generally conservative behavior. *Geochim. Cosmochim. Acta* **1992**, *56*, 4099–4103. [[CrossRef](#)]
- Crusius, J.; Calvert, S.; Pedersen, T.; Sage, D. Rhenium and molybdenum enrichments in sediments as indicators of oxic, suboxic and sulfidic conditions of deposition. *Earth Planet. Sci. Lett.* **1996**, *145*, 65–78. [[CrossRef](#)]
- Kendall, B.; Reinhard, C.T.; Lyons, T.W.; Kaufman, A.J.; Poulton, S.W.; Anbar, A.D. Pervasive oxygenation along late Archaean ocean margins. *Nat. Geosci.* **2010**, *3*, 647–652. [[CrossRef](#)]
- Planavsky, N.J.; Slack, J.F.; Cannon, W.F.; O’Connell, B.; Isson, T.T.; Asael, D.; Jackson, J.C.; Hardisty, D.S.; Lyons, T.W.; Bekker, A. Evidence for episodic oxygenation in a weakly redox-buffered deep mid-Proterozoic ocean. *Chem. Geol.* **2018**, *483*, 581–594. [[CrossRef](#)]
- Sheen, A.I.; Kendall, B.; Reinhard, C.T.; Creaser, R.A.; Lyons, T.W.; Bekker, A.; Poulton, S.W.; Anbar, A.D. A model for the oceanic mass balance of rhenium and implications for the extent of Proterozoic ocean anoxia. *Geochim. Cosmochim. Acta* **2018**, *227*, 75–95. [[CrossRef](#)]
- Bennett, W.W.; Canfield, D.E. Redox-sensitive trace metals as paleoredox proxies: A review and analysis of data from modern sediments. *Earth-Sci. Rev.* **2020**, *204*, 103175. [[CrossRef](#)]
- Helz, G.R. The Re/Mo redox proxy reconsidered. *Geochim. Cosmochim. Acta* **2022**, *317*, 507–522. [[CrossRef](#)]
- Langmuir, D. *Aqueous Environmental Geochemistry*; Prentice-Hall, Inc.: Upper Saddle River, NJ, USA, 1997; p. 600.
- Thamdrup, B. Bacterial manganese and iron reduction in aquatic sediments. *Adv. Microb. Ecol.* **2000**, *16*, 41–84.
- Amonette, J.E. Iron redox chemistry of clays and oxides: Environmental applications. In *Electrochemical Properties of Clays*; Fitch, A., Ed.; The Clay Minerals Society: Aurora, CO, USA, 2002; Volume 10, pp. 89–147.
- Wagmann, D.D.; Evans, W.H.; Parker, V.B.; Schumm, R.H.; Halow, I.; Bailey, S.M.; CHurney, K.L.; Nuttall, R.L. *The NBS Tables of Chemical Thermodynamic Properties*; American Chemical Society and The American Institute of Physics: New York, NY, USA, 1982.
- Rard, J.A.; Rand, M.H.; Anderegg, G.; Wanner, H. *Chemical Thermodynamics of Technetium*; Elsevier: New York, NY, USA, 1999.
- Morford, J.L.; Martin, W.R.; Carney, C.M. Rhenium geochemical cycling: Insights from continental margins. *Chem. Geol.* **2012**, *324–325*, 73–86. [[CrossRef](#)]
- Helz, G.R.; Dolor, M.K. What regulates rhenium deposition in euxinic basins? *Chem. Geol.* **2012**, *304–305*, 131–141. [[CrossRef](#)]
- Anbar, A.D.; Duan, Y.; Lyons, T.W.; Arnold, G.L.; Kendall, B.; Creaser, R.A.; Kaufman, A.J.; Gordon, G.W.; Scott, C.; Garvin, J.; et al. A whiff of oxygen before the great oxidation event? *Science* **2007**, *317*, 1903–1906. [[CrossRef](#)]
- Jaffe, L.A.; Peucker-Ehrenbrink, B.; Petsch, S.T. Mobility of rhenium, platinum group elements and organic carbon during black shale weathering. *Earth Planet. Sci. Lett.* **2002**, *198*, 339–353. [[CrossRef](#)]
- Gadd, G.M. Metals, minerals and microbes: Geomicrobiology and bioremediation. *Microbiology* **2010**, *156*, 609–643. [[CrossRef](#)] [[PubMed](#)]

25. Icenhower, J.P.; Qafoku, N.P.; Zachara, J.M.; Martin, W.J. The biogeochemistry of technetium: A review of the behavior of an artificial element in the natural environment. *Am. J. Sci.* **2011**, *310*, 721–752. [[CrossRef](#)]
26. Dolor, M.K.; Gilmour, C.C.; Helz, G.R. Distinct microbial behavior of Re compared to Tc: Evidence against microbial Re fixation in aquatic sediments. *Geomicrobiol. J.* **2009**, *26*, 470–483. [[CrossRef](#)]
27. Lloyd, J.R.; Ridley, J.; Khizniak, T.; Lyalikova, N.N.; MaCaskie, L.E. Reduction of technetium by Desulfovibrio desulfuricans: Biocatalyst characterization and use in a flowthrough bioreactor. *Appl. Environ. Microbiol.* **1999**, *65*, 2691–2696. [[CrossRef](#)] [[PubMed](#)]
28. Liu, C.; Gorby, Y.A.; Zachara, J.M.; Fredrickson, J.K.; Brown, C.F. Reduction kinetics of Fe(III), Co(III), U(VI), Cr(VI), and Tc(VII) in cultures of dissimilatory metal-reducing bacteria. *Biotechnol. Bioeng.* **2002**, *80*, 637–649. [[CrossRef](#)] [[PubMed](#)]
29. O’Loughlin, E.J.; Boyanov, M.I.; Antonopoulos, D.A.; Kemner, K.M. Redox processes affecting the speciation of technetium, uranium, neptunium, and plutonium in aquatic and terrestrial environments. In *Aquatic Redox Processes*; Tratnyek, P.G., Grundl, T.J., Haderlein, S.B., Eds.; American Chemical Society: Washington, DC, USA, 2011; Volume 1071, pp. 477–517.
30. Wharton, M.J.; Atkins, B.; Charnock, J.M.; Livens, F.R.; Patrick, R.A.D.; Collison, D. An X-ray absorption spectroscopy study of the coprecipitation of Tc and Re with mackinawite (FeS). *Appl. Geochem.* **2000**, *15*, 347–354. [[CrossRef](#)]
31. Ding, Q.; Ding, F.; Qian, T.; Zhao, D.; Wang, L. Reductive Immobilization of Rhenium in Soil and Groundwater Using Pyrite Nanoparticles. *Water Air Soil Pollut.* **2015**, *226*, 409. [[CrossRef](#)]
32. Wang, T.; Qian, T.; Zhao, D.; Liu, X.; Ding, Q. Immobilization of perrhenate using synthetic pyrite particles: Effectiveness and remobilization potential. *Sci. Total Environ.* **2020**, *725*, 138423. [[CrossRef](#)]
33. Usman, M.; Byrne, J.M.; Chaudhary, A.; Orsetti, S.; Hanna, K.; Ruby, C.; Kappler, A.; Haderlein, S.B. Magnetite and Green Rust: Synthesis, Properties, and Environmental Applications of Mixed-Valent Iron Minerals. *Chem. Rev.* **2018**, *118*, 3251–3304. [[CrossRef](#)]
34. Huang, J.; Jones, A.; Waite, T.D.; Chen, Y.; Huang, X.; Rosso, K.M.; Kappler, A.; Mansor, M.; Tratnyek, P.G.; Zhang, H. Fe(II) Redox Chemistry in the Environment. *Chem. Rev.* **2021**, *121*, 8161–8233. [[CrossRef](#)]
35. Kappler, A.; Bryce, C.; Mansor, M.; Lueder, U.; Byrne, J.M.; Swanner, E.D. An evolving view on biogeochemical cycling of iron. *Nat. Rev. Microbiol.* **2021**, *19*, 360–374. [[CrossRef](#)]
36. Boyanov, M.I.; Kemner, K.M. Application of synchrotron X-ray absorption spectroscopy and microscopy techniques to the study of biogeochemical processes. In *Analytical Geomicrobiology: A Handbook of Instrumental Techniques*; Kenney, J.P.L., Veeramani, H., Alessi, D.S., Eds.; Cambridge University Press: Cambridge, UK, 2019; pp. 238–261. [[CrossRef](#)]
37. Johnson, C.R.; Antonopoulos, D.A.; Boyanov, M.I.; Flynn, T.M.; Koval, J.C.; Kemner, K.M.; O’Loughlin, E.J. Reduction of Sb(V) by coupled biotic-abiotic processes under sulfidogenic conditions. *Heliyon* **2021**, *7*, e06275. [[CrossRef](#)]
38. O’Loughlin, E.J.; Boyanov, M.I.; Kemner, K.M.; Thalhammer, K.O. Reduction of Hg(II) by Fe(II)-bearing smectite clay minerals. *Minerals* **2020**, *10*, 1079. [[CrossRef](#)]
39. Kropf, A.J.; Katsoudas, J.; Chattopadhyay, S.; Shibata, T.; Lang, E.A.; Zyryanov, V.N.; Ravel, B.; McIvor, K.; Kemner, K.M.; Scheckel, K.G.; et al. The new MRCAT (Sector 10) bending magnet beamline at the Advanced Photon Source. *AIP Conf. Proc.* **2010**, *1234*, 299–302. [[CrossRef](#)]
40. Choe, J.K.; Boyanov, M.I.; Liu, J.; Kemner, K.M.; Werth, C.J.; Strathmann, T.J. X-ray Spectroscopic Characterization of Immobilized Rhenium Species in Hydrated Rhenium–Palladium Bimetallic Catalysts Used for Perchlorate Water Treatment. *J. Phys. Chem. C* **2014**, *118*, 11666–11676. [[CrossRef](#)]
41. Dickson, J.; Conroy, N.A.; Xie, Y.; Powell, B.A.; Seaman, J.C.; Boyanov, M.I.; Kemner, K.M.; Kaplan, D.I. Surfactant-modified siliceous zeolite Y for pertechnetate remediation. *Chem. Eng. J.* **2020**, *402*, 126268. [[CrossRef](#)]
42. Ankudinov, A.L.; Ravel, B.; Conradson, S.D. Real-space multiple-scattering calculation and interpretation of X-ray absorption near-edge structure. *Phys. Rev. B* **1998**, *58*, 7565–7576. [[CrossRef](#)]
43. Newville, M.; Ravel, B.; Haskel, D.; Stern, E.A. Analysis of multiple scattering XAFS data using theoretical standards. *Phys. B* **1995**, *208/209*, 154–156. [[CrossRef](#)]
44. Corrêa, H.P.S.; Cavalcante, I.P.; Martinez, L.G.; Orlando, C.G.P.; Orlando, M.T.D. Refinement of monoclinic ReO_2 structure from XRD by Rietveld method. *Braz. J. Phys.* **2004**, *34*, 1208–1210. [[CrossRef](#)]
45. Fung, A.S.; Kelley, M.J.; Koningsberger, D.C.; Gates, B.C. $\gamma\text{-Al}_2\text{O}_3$ -Supported Re–Pt Cluster Catalyst Prepared from [Re₂Pt(CO)₁₂]: Characterization by Extended X-ray Absorption Fine Structure Spectroscopy and Catalysis of Methylcyclohexane Dehydrogenation. *J. Am. Chem. Soc.* **1997**, *119*, 5877–5887. [[CrossRef](#)]
46. Chaudhuri, S.K.; Lack, J.G.; Coates, J.D. Biogenic magnetite formation through anaerobic biooxidation of Fe(II). *Appl. Environ. Microbiol.* **2001**, *67*, 2844–2848. [[CrossRef](#)]
47. Pantke, C.; Obst, M.; Benzerara, K.; Morin, G.; Ona-Nguema, G.; Dippon, U.; Kappler, A. Green rust formation during Fe(II) oxidation by the nitrate-reducing Acidovorax sp. strain BoFeN1. *Environ. Sci. Technol.* **2012**, *46*, 1439–1446. [[CrossRef](#)]
48. Etique, M.; Jorand, F.P.; Zegeye, A.; Gregoire, B.; Despas, C.; Ruby, C. Abiotic process for Fe(II) oxidation and green rust mineralization driven by a heterotrophic nitrate reducing bacteria (*Klebsiella mobilis*). *Environ. Sci. Technol.* **2014**, *48*, 3742–3751. [[CrossRef](#)]
49. Nordhoff, M.; Tominski, C.; Halama, M.; Byrne, J.M.; Obst, M.; Kleindienst, S.; Behrens, S.; Kappler, A. Insights into nitrate-reducing Fe(II) oxidation mechanisms through analysis of cell-mineral associations, cell encrustation, and mineralogy in the chemolithoautotrophic enrichment culture KS. *Appl. Environ. Microbiol.* **2017**, *83*, e00752-17. [[CrossRef](#)] [[PubMed](#)]

50. Fredrickson, J.K.; Zachara, J.M.; Kennedy, D.W.; Dong, H.; Onstott, T.C.; Hinman, N.W.; Li, S.-M. Biogenic iron mineralization accompanying the dissimilatory reduction of hydrous ferric oxide by a groundwater bacterium. *Geochim. Cosmochim. Acta* **1998**, *62*, 3239–3257. [[CrossRef](#)]
51. Hansel, C.M.; Benner, S.G.; Neiss, J.; Dohnalkova, A.; Kukkadapu, R.K.; Fendorf, S. Secondary mineralization pathways induced by dissimilatory iron reduction of ferrihydrite under advective flow. *Geochim. Cosmochim. Acta* **2003**, *67*, 2977–2992. [[CrossRef](#)]
52. Borch, T.; Masue, Y.; Kukkadapu, R.K.; Fendorf, S. Phosphate imposed limitations on biological reduction and alteration of ferrihydrite. *Environ. Sci. Technol.* **2007**, *41*, 166–172. [[CrossRef](#)] [[PubMed](#)]
53. Shimizu, M.; Zhou, J.; Schröder, C.; Obst, M.; Kappler, A.; Borch, T. Dissimilatory reduction and transformation of ferrihydrite-humic acid coprecipitates. *Environ. Sci. Technol.* **2013**, *47*, 13375–13384. [[CrossRef](#)] [[PubMed](#)]
54. Ona-Nguema, G.; Abdelmoula, M.; Jorand, F.; Benali, O.; Géhin, A.; Block, J.-C.; Génin, J.-M.R. Iron(II,III) hydroxycarbonate green rust formation and stabilization from lepidocrocite bioreduction. *Environ. Sci. Technol.* **2002**, *36*, 16–20. [[CrossRef](#)] [[PubMed](#)]
55. Jorand, F.; Zegeye, A.; Landry, F.; Ruby, C. Reduction of ferric green rust by Shewanella putrefaciens. *Lett. Appl. Microbiol.* **2007**, *45*, 515–521. [[CrossRef](#)]
56. Jung, J.; Bae, S.; Lee, W. Indirect contact of bio-transformation of lepidocrocite: Role of electron transfer mediator. *Sustain. Environ. Res.* **2012**, *23*, 193–198.
57. Boyanov, M.I.; O'Loughlin, E.J.; Kemner, K.M. Iron phase transformations resulting from the respiration of Shewanella putrefaciens on a mixed mineral phase. *J. Phys. Conf. Ser.* **2009**, *190*, 012193. [[CrossRef](#)]
58. O'Loughlin, E.J.; Boyanov, M.I.; Flynn, T.M.; Gorski, C.; Hofmann, S.M.; McCormick, M.L.; Scherer, M.M.; Kemner, K.M. Effects of bound phosphate on the bioreduction of lepidocrocite (g-FeOOH) and maghemite ($\text{g-Fe}_2\text{O}_3$) and formation of secondary minerals. *Environ. Sci. Technol.* **2013**, *47*, 9157–9166. [[CrossRef](#)]
59. Dong, Y.; Sanford, R.A.; Boyanov, M.I.; Flynn, T.M.; O'Loughlin, E.J.; Kemner, K.M.; George, S.; Fouke, K.E.; Li, S.; Huang, D.; et al. Controls on iron reduction and biomimetic mineralization over broad environmental conditions as suggested by the Firmicutes Orenia metallireducens strain Z6. *Environ. Sci. Technol.* **2020**, *54*, 10128–10140. [[CrossRef](#)]
60. O'Loughlin, E.J.; Boyanov, M.I.; Gorski, C.A.; Scherer, M.M.; Kemner, K.M. Effects of Fe(III) oxide mineralogy and phosphate on Fe(II) secondary mineral formation during microbial iron reduction. *Minerals* **2021**, *11*, 149. [[CrossRef](#)]
61. Bigham, J.M.; Tuovinen, O.H. Mineralogical, morphological, and microbiological characteristics of tubercles in cast iron water mains as related to their chemical activity. In *Planetary Ecology*; Caldwell, D.E., Brierley, J.A., Brierley, C.L., Eds.; Van Nostrand Reinhold Co.: New York, NY, USA, 1985; pp. 239–250.
62. Génin, J.-M.R.; Refait, P.; Olowe, A.A.; Abdelmoula, M.; Fall, I.; Drissi, S.H. Identification of green rust compounds in the aqueous corrosion processes of steels; the case of microbially induced corrosion and use of 78 K CEMS. *Hyperfine Interact.* **1998**, *112*, 47–50. [[CrossRef](#)]
63. Kumar, A.V.R.; Singh, R.; Nigam, R.K. Mössbauer spectroscopy of corrosion products of mild steel due to microbiologically influenced corrosion. *J. Radioanal. Nucl. Chem.* **1999**, *242*, 131–137. [[CrossRef](#)]
64. Refait, P.; Abdelmoula, M.; Génin, J.-M.R. Mechanisms of formation and structure of green rust one in aqueous corrosion of iron in the presence of chloride ions. *Corros. Sci.* **1998**, *40*, 1547–1560. [[CrossRef](#)]
65. Hansen, H.C.B.; Bender Koch, C.; Nancke-Krogh, H.; Borggaard, O.K.; Sørensen, J. Abiotic nitrate reduction to ammonium: Key role of green rust. *Environ. Sci. Technol.* **1996**, *30*, 2053–2056. [[CrossRef](#)]
66. Christiansen, B.C.; Geckes, H.; Marquardt, C.M.; Bauer, A.; Römer, J.; Wiss, T.; Schild, D.; Stipp, S.L.S. Neptunyl (NpO_2^+) interaction with green rust, $\text{GR}_{\text{Na},\text{SO}_4}$. *Geochim. Cosmochim. Acta* **2011**, *75*, 1216–1226. [[CrossRef](#)]
67. Heasman, D.M.; Sherman, D.M.; Ragnarsdóttir, K.V. The reduction of aqueous Au^{3+} by sulfide minerals and green rust phases. *Am. Mineral.* **2003**, *88*, 725–738. [[CrossRef](#)]
68. Myneni, S.C.B.; Tokunaga, T.K.; Brown, G.E., Jr. Abiotic selenium redox transformations in the presence of Fe(II,III) oxides. *Science* **1997**, *278*, 1106–1109. [[CrossRef](#)]
69. O'Loughlin, E.J.; Kelly, S.D.; Kemner, K.M.; Csencsits, R.; Cook, R.E. Reduction of Ag^{I} , Au^{III} , Cu^{II} , and Hg^{II} by $\text{Fe}^{\text{II}}/\text{Fe}^{\text{III}}$ hydroxysulfate green rust. *Chemosphere* **2003**, *53*, 437–446. [[CrossRef](#)]
70. Pepper, S.E.; Bunker, D.J.; Bryan, N.D.; Livens, F.R.; Charnock, J.M.; Patrick, R.A.D.; Collison, D. Treatment of radioactive wastes: An X-ray adsorption spectroscopy study of the treatment of technetium with green rust. *J. Colloid Interface Sci.* **2003**, *268*, 408–412. [[CrossRef](#)]
71. Choi, J.; Lee, W. Enhanced degradation of tetrachloroethylene by green rusts with platinum. *Environ. Sci. Technol.* **2008**, *42*, 3356–3362. [[CrossRef](#)]
72. Refait, P.; Simon, L.; Génin, J.-M.R. Reduction of SeO_4^{2-} anions and anoxic formation of iron(II)-iron(III) hydroxy-selenate green rust. *Environ. Sci. Technol.* **2000**, *34*, 819–825. [[CrossRef](#)]
73. Williams, A.G.B.; Scherer, M.M. Kinetics of Cr(VI) reduction by carbonate green rust. *Environ. Sci. Technol.* **2001**, *35*, 3488–3494. [[CrossRef](#)]
74. Yan, S.; Boyanov, M.I.; Mishra, B.; Kemner, K.M.; O'Loughlin, E.J. U(VI) reduction by biogenic and abiotic hydroxycarbonate green rusts: Impacts on U(IV) speciation and stability over time. *Environ. Sci. Technol.* **2018**, *52*, 4601–4609. [[CrossRef](#)] [[PubMed](#)]
75. O'Loughlin, E.J.; Boyanov, M.I.; Kemner, K.M. Reduction of vanadium(V) by iron(II)-bearing minerals. *Minerals* **2021**, *11*, 316. [[CrossRef](#)]

76. Zhang, Z.; Yan, W.; Messan, O.; Fang, J.; Jackson, W.A. Abiotic Reduction of Nitrate and Chlorate by Green Rust. *ACS Earth Space Chem.* **2021**, *5*, 2042–2051. [[CrossRef](#)]
77. O'Loughlin, E.J.; Boyanov, M.I.; Kemner, K.M. Tellurium goes for a ride on the “Ferrous” Wheel: Interactions of Te(VI) and Te(IV) with iron(II)-bearing minerals. *ACS Earth Space Chem.* **2023**, *7*, 1825–1836. [[CrossRef](#)]
78. Zhang, X.; Jia, Q.; Deng, J.; Li, L.; Dai, Y.; Zhu, L.; Huang, L.-Z. Intervention timing of H^{*} and •OH determines the catalytical degradation of tribromophenol by palladium(II) doped green rust in redox-alternating environments. *Appl. Catal. B Environ.* **2024**, *343*, 123510. [[CrossRef](#)]
79. Brookins, D.G. Rhenium as analog for fissionogenic technetium: Eh-pH diagram (25 °C, 1 bar) constraints. *Appl. Geochem.* **1986**, *1*, 513–517. [[CrossRef](#)]
80. Kim, E.; Boulègue, J. Chemistry of rhenium as an analogue of technetium: Experimental studies of the dissolution of rhenium oxides in aqueous solutions. *Radiochim. Acta* **2003**, *91*, 211–216. [[CrossRef](#)]
81. Wakoff, B.; Nagy, K.L. Perrhenate uptake by iron and aluminum oxyhydroxides: An analogue for pertechnetate incorporation in Hanford waste tank sludges. *Environ. Sci. Technol.* **2004**, *38*, 1765–1771. [[CrossRef](#)] [[PubMed](#)]
82. Duckworth, S.; Gaona, X.; Castaño, D.; Park, S.; Altmaier, M.; Geckeis, H. Redox chemistry, solubility and hydrolysis of Re in reducing aquatic systems. Thermodynamic description and comparison with Tc. *Appl. Geochem.* **2021**, *132*, 105037. [[CrossRef](#)]
83. Meena, A.H.; Arai, Y. Environmental geochemistry of technetium. *Environ. Chem. Lett.* **2017**, *15*, 241–263. [[CrossRef](#)]
84. Pearce, C.I.; Icenhower, J.P.; Asmussen, R.M.; Tratnyek, P.G.; Rosso, K.M.; Lukens, W.W.; Qafoku, N.P. Technetium Stabilization in Low-Solubility Sulfide Phases: A Review. *ACS Earth Space Chem.* **2018**, *2*, 532–547. [[CrossRef](#)]
85. Wang, J.; Xu, B. Removal of radionuclide (99)Tc from aqueous solution by various adsorbents: A review. *J. Environ. Radioact.* **2023**, *270*, 107267. [[CrossRef](#)]
86. Cui, D.; Eriksen, T.E. Reduction of pertechnetate in solution by heterogeneous electron transfer from Fe(II)-containing geological material. *Environ. Sci. Technol.* **1996**, *30*, 2263–2269. [[CrossRef](#)]
87. Kobayashi, A.; Ogra, Y. Metabolism of tellurium, antimony and germanium simultaneously administered to rats. *J. Toxicol. Sci.* **2009**, *34*, 295–303. [[CrossRef](#)]
88. Yalcintas, E.; Scheinost, A.C.; Gaona, X.; Altmaier, M. Systematic XAS study on the reduction and uptake of Tc by magnetite and mackinawite. *Dalton Trans.* **2016**, *45*, 17874–17885. [[CrossRef](#)]
89. McBeth, J.M.; Lloyd, J.R.; Law, G.T.W.; Livens, F.R.; Burke, I.T.; Morris, K. Redox interactions of technetium with iron-bearing minerals. *Mineral. Mag.* **2018**, *75*, 2419–2430. [[CrossRef](#)]
90. Jaisi, D.P.; Dong, H.; Plymale, A.E.; Frederickson, J.K.; Zachara, J.M.; Heald, S.; Liu, C. Reduction and longterm immobilization of technetium by Fe(II) associated with clay mineral nontronite. *Chem. Geol.* **2009**, *264*, 127–138. [[CrossRef](#)]
91. Yang, J.; Kukkadapu, R.K.; Dong, H.; Shelobolina, E.S.; Zhang, J.; Kim, J. Effects of redox cycling of iron in nontronite on reduction of technetium. *Chem. Geol.* **2012**, *291*, 206–216. [[CrossRef](#)]
92. Livens, F.R.; Jones, M.J.; Hynes, A.J.; Charnock, J.M.; Mosselmans, J.F.W.; Hennig, C.; Steele, H.; Collison, D.; Vaughan, D.J.; Patrick, R.A.D.; et al. X-ray adsorption spectroscopy studies of reactions of technetium, uranium and neptunium with mackinawite. *J. Environ. Radioact.* **2004**, *74*, 211–219. [[CrossRef](#)]
93. Bruggeman, C.; Maes, A.; Vancluysen, J. The identification of FeS₂ as a sorption sink for Tc(IV). *Phys. Chem. Earth Parts A/B/C* **2007**, *32*, 573–580. [[CrossRef](#)]
94. Rodriguez, D.M.; Mayordomo, N.; Scheinost, A.C.; Schild, D.; Brendler, V.; Muller, K.; Stumpf, T. New Insights into (99)Tc(VII) Removal by Pyrite: A Spectroscopic Approach. *Environ. Sci. Technol.* **2020**, *54*, 2678–2687. [[CrossRef](#)]
95. Maset, E.R.; Sidhu, S.H.; Fisher, A.; Heydon, A.; Worsfold, P.J.; Cartwright, A.J.; Keith-Roach, M.J. Effect of organic co-contaminants on technetium and rhenium speciation and solubility under reducing conditions. *Environ. Sci. Technol.* **2006**, *40*, 5472–5477. [[CrossRef](#)] [[PubMed](#)]
96. Heald, S.M.; Krupka, K.M.; Brown, C.F. Incorporation of pertechnetate and perrenate into corroded steel surfaces studied by X-ray absorption fine structure spectroscopy. *Radiochim. Acta* **2012**, *100*, 243–253. [[CrossRef](#)]
97. Li, D.; Seaman, J.C.; Hunyadi Murph, S.E.; Kaplan, D.I.; Taylor-Pashow, K.; Feng, R.; Chang, H.; Tandukar, M. Porous iron material for TcO(4)- and ReO(4)- sequestration from groundwater under ambient oxic conditions. *J. Hazard. Mater.* **2019**, *374*, 177–185. [[CrossRef](#)] [[PubMed](#)]
98. Halevy, I.; Alesker, M.; Schuster, E.M.; Popovitz-Biro, R.; Feldman, Y. A key role for green rust in the Precambrian oceans and the genesis of iron formations. *Nat. Geosci.* **2017**, *10*, 135–139. [[CrossRef](#)]
99. Russell, M.J. Green Rust: The Simple Organizing ‘Seed’ of All Life? *Life* **2018**, *8*, 35. [[CrossRef](#)]
100. Duval, S.; Branscomb, E.; Trolard, F.; Bourrié, G.; Grauby, O.; Heresanu, V.; Schoepp-Cothenet, B.; Zuchan, K.; Russell, M.J.; Nitschke, W. On the why’s and how’s of clay minerals’ importance in life’s emergence. *Appl. Clay Sci.* **2020**, *195*, 105737. [[CrossRef](#)]
101. Poulton, S.W.; Canfield, D.E. Ferruginous Conditions: A Dominant Feature of the Ocean through Earth’s History. *Elements* **2011**, *7*, 107–112. [[CrossRef](#)]

102. Crusius, J.; Thomson, J. Comparative behavior of authigenic Re, U, and Mo during reoxidation and subsequent long-term burial in marine sediments. *Geochim. Cosmochim. Acta* **2000**, *64*, 2233–2242. [[CrossRef](#)]
103. Sundby, B.; Martinez, P.; Gobeil, C. Comparative geochemistry of cadmium, rhenium, uranium, and molybdenum in continental margin sediments. *Geochim. Cosmochim. Acta* **2004**, *68*, 2485–2493. [[CrossRef](#)]

Disclaimer/Publisher's Note: The statements, opinions and data contained in all publications are solely those of the individual author(s) and contributor(s) and not of MDPI and/or the editor(s). MDPI and/or the editor(s) disclaim responsibility for any injury to people or property resulting from any ideas, methods, instructions or products referred to in the content.